Analysis of the R_0A product and detectivity in a GaInAsSb infrared photovoltaic detector

1998 J. Phys. D: Appl. Phys. 31 3291

(http://iopscience.iop.org/0022-3727/31/22/018)

J. Phys. D: Appl. Phys. **31** (1998) 3291–3297. Printed in the UK PII: S0022-3727(98)93495-7

Analysis of the R_0A product and detectivity in a GaInAsSb infrared photovoltaic detector

Yuan Tian†, Tianming Zhou, Baolin Zhang, Yixin Jin and Hong Jiang

Changchun Institute of Physics, Chinese Academy of Sciences, Changchun 130021, People's Republic of China

Received 21 April 1998, in final form 26 June 1998

Abstract. In this paper a theoretical analysis of the R_0A product and the detectivity in a GaInAsSb infrared photovoltaic detector is reported, dependent on the four fundamental kinds of noise mechanism and the quantum efficiency. The considerations are carried out for near room temperature and 2.5 μm wavelength. The analytical results show that the noise mechanisms can be reduced, and correspondingly the performance of such detectors can be improved.

1. Introduction

Modern high-performance infrared photovoltaic detector technology, based on photon absorption in narrow-gap semiconductors, requires the use of extensive detector cooling to achieve background limited performances (BLIP) [1, 2]. Cooling is an effective but rather impractical way to suppress noise because cryogenic cooling makes detectors bulky and inconvenient in use. Infrared detectors working near room temperature have been fabricated by the MOCVD technique [3, 4] and moreover, theoretical results indicate that such detectors can also obtain high performance.

In this paper, theoretical analysis is explored for room-temperature operation of infrared (IR) photovoltaic (PV) detectors based on bulk $Ga_xIn_{1-x}As_{1-y}Sb_y$ alloys lattice-matched to GaSb, which have become very important materials in recent years in the fabrication of detectors designed for 2–4 μm infrared wavelength applications [3–5]. The current passing the contacts of a device causes noise because of the statistical nature of the generation and recombination processes. In general, the detectivity D^* is the main parameter characterizing normalized signal-to-noise performance of the detectors. The aim is to suppress all kinds of noise and to improve the detectivity. Numerous theoretical discussions of the zero-bias resistance–junction area R_0A product and the detectivity D^*, which are figures of merit commonly used to characterize IR PV detectors, are carried out dependent on design material parameters for prediction and achievement of detector performance. There are four fundamental kinds of noise mechanism in IR PV detectors. In most reports, authors have paid much attention to analysing the effect of the Auger mechanism (one kind of role in the diffusion current) on the R_0A product and the detectivity of photodetectors [6–8], even though other original currents may exist in different physical mechanisms, such as radiative recombination (the other kind of role in the diffusion current) in the n and p neutral regions, generation–recombination (G–R) in the depletion region and tunnelling through the p–n junction [9, 10]. In this paper, the influence of the above junction current components on the R_0A product and the detectivity of an n–p GaInAsSb IR PV detector is considered. In addition, the quantum efficiency is considered. These results show much difference from those that are obtained when only the Auger mechanism is considered in a GaInAsSb IR PV detector [8].

2. Theoretical analysis

For the purposes of discussion, the structure of the GaInAsSb detector can be simplified as a p–n junction structure. Four kinds of noise mechanism are considered with the total R_0A product $(R_0A)_{\mathrm{total}}$ and the detectivity D^*, where the relation between D^* and $(R_0A)_{\mathrm{total}}$ is [11]

$$D^* = \frac{q\eta\lambda}{hc}\sqrt{\frac{R_0A}{4KT}} \tag{1}$$

where η and T are the quantum efficiency and working temperature in a detector, λ is the incident light wavelength and q and k are constants with their usual meaning.

Because all the noise mechanisms are independent, $(R_0A)_{\mathrm{total}}$ is expressed by

$$\frac{1}{(R_0A)_{\mathrm{total}}} = \frac{1}{(R_0A)_{\mathrm{Auger}}} + \frac{1}{(R_0A)_{\mathrm{rad}}} + \frac{1}{(R_0A)_{\mathrm{GR}}} + \frac{1}{(R_0A)_{\mathrm{tunnel}}} \tag{2}$$

† E-mail address: snmocvd@public.cc.jl.cn

0022-3727/98/223291+07$19.50

where $(R_0A)_{\mathrm{Auger}}$, $(R_0A)_{\mathrm{rad}}$, $(R_0A)_{\mathrm{GR}}$ and $(R_0A)_{\mathrm{tunnel}}$ denote the Auger, radiative, G–R and tunnel mechanisms respectively.

2.1. The Auger mechanism and radiative mechanism

The diffusion current that is the fundamental current in a p–n junction detector determines $(R_0A)_{\mathrm{Auger}}$ and $(R_0A)_{\mathrm{rad}}$, shown as follows [12]

$$(R_0A)_j = \frac{KT}{q^2}\left[\frac{D_p n}{L_p n_i^2}\frac{r_p\cosh(\frac{t-x_n}{L_p})+\sinh(\frac{t-x_n}{L_p})}{r_p\sinh(\frac{t-x_n}{L_p})+\cosh(\frac{t-x_n}{L_p})} + \frac{D_e p}{L_e n_i^2}\frac{r_e\cosh(\frac{d-x_p}{L_e})+\sinh(\frac{d-x_p}{L_e})}{r_e\sinh(\frac{d-x_p}{L_e})+\cosh(\frac{t-x_p}{L_e})}\right] \qquad (3)$$

$$D_i = KT\mu_i/q,\ L_i = (D_i\tau_i)^{1/2},\ \gamma_i = L_iS_i/D_i (i = n \text{ or } p)$$

D_i, L_i, μ_i, S_i and τ_i are the diffusion coefficient (cm^2 s^{-1}), diffusion length (cm), effective mobility (cm^2 V^{-1} s^{-1}), surface recombination velocity (m s^{-1}) and carrier lifetime (s) respectively for holes in the n region or for electrons in the p region. p or n is the major carrier concentration (cm^{-3}) in those respective regions; n_i is the intrinsic carrier concentration (cm^{-3}).

In equation (3), $(R_0A)_j$ is embodied by minority lifetimes of the Auger mechanism $(R_0A)_{\mathrm{Auger}}$ or the radiative mechanism $(R_0A)_{\mathrm{rad}}$ in both of which the Auger lifetime has been calculated by many authors [8–10]. The radiative lifetime is given by [13, 14]

$$\tau_R^h = \frac{1}{B[n+(n_i^2/n)]} \text{ (in the n region)} \qquad (4a)$$

$$\tau_R^e = \frac{1}{B[p+(n_i^2/p)]} \text{ (in the p region)} \qquad (4b)$$

where τ_R^h, τ_R^e are the radiative lifetimes for holes in the n region and for electrons in the p region. B is a constant defined by

$$B = 5.8\times10^{-13}\varepsilon_\infty^{1/2}\left(\frac{1}{m_e^*+m_h^*}\right)^{3/2}\left(1+\frac{1}{m_e^*}+\frac{1}{m_h^*}\right)\times(300/T)^{3/2}E_g^2 \qquad (4c)$$

where $\varepsilon_\infty = 14$, the high-frequency dielectric constant, and m_e^*, m_h^* are the electron or hole effective mass; E_g is the GaInAsSb bandgap energy.

2.2. The generation–recombination mechanism

The third type of fundamental noise component appears in the space-charge region and is called the G–R (generation–recombination) mechanism, which is caused by lattice defects and impurities in the forbidden energy gap of a semiconductor. The R_0A product associated with the G–R current is equal to [15]

$$(R_0A)_{\mathrm{GR}} = \frac{\sqrt{\tau_{n0}\tau_{p0}}V_{bi}}{qn_iwf(b)} \qquad (5a)$$

where τ_{n0}, τ_{p0} are the electron and hole lifetimes within the depletion region, w is the width of the depletion region and V_{bi} is the built-in voltage through the p–n junction.

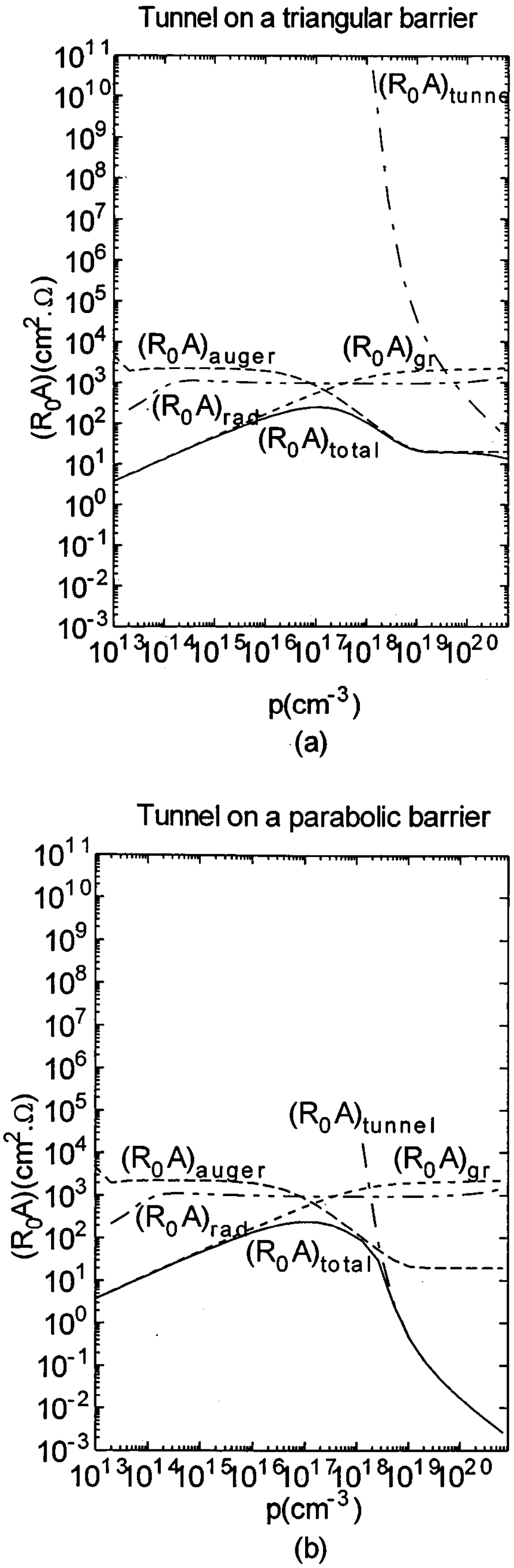

Figure 1. The dependence of $(R_0A)_{\mathrm{total}}$ and the R_0A product components on the p-side carrier concentration (p) for tunnelling (a) on a triangular barrier and (b) for a parabolic barrier: $t = 0.5$ μm, $d = 5$ μm, $S_e = S_p = 0$, $n = 10^{18}$ cm^{-3}, $\sigma N_f = 0.1$ cm^{-1}, $\mu_e = 1000$ cm^2 V^{-1} s^{-1} and $\mu_p = 240$ cm^2 V^{-1} s^{-1}.

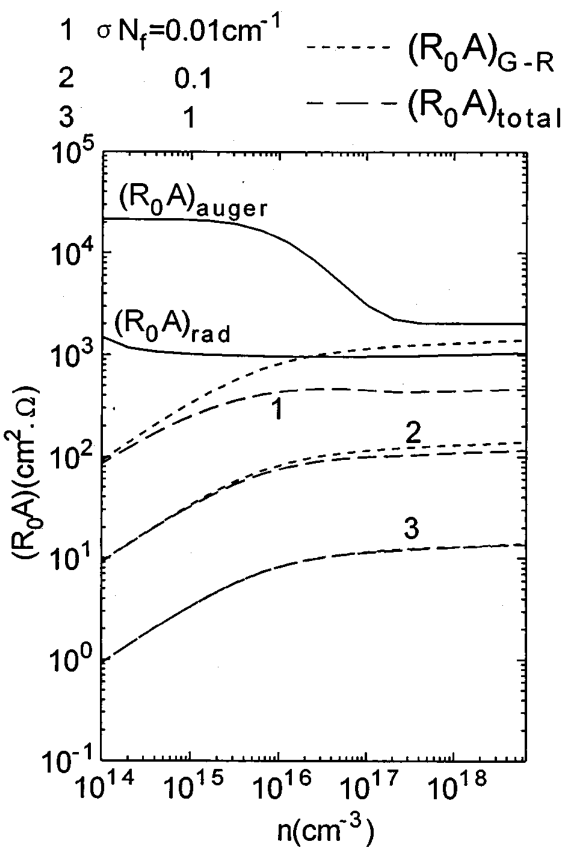

Figure 2. The dependence of $(R_0A)_{\text{total}}$ and the R_0A product components on the n-side carrier concentration (n) with the σN_f product as a parameter: $t = 0.5$ μm, $d = 5$ μm, $S_e = S_p = 0$, $p = 6.4 \times 10^{15}$ cm^{-3}, $\mu_e = 1000$ cm^2 V^{-1} s^{-1} and $\mu_p = 240$ cm^2 V^{-1} s^{-1}.

The function $f(b)$ is a definite integral depending on the position of recombination centres in the energy gap. For simplicity, we further assume $f(b) = 1$, and $\tau_{n0} = \tau_{p0} = \tau_0 = 1/V_{th}\sigma N_f$ [16], where $V_{th} = (3KT/m^*)^{1/2}$ (m^* being the effective mass), σ is the capture cross section and N_f is the trap density. In this relationship, we assume that σ and N_f for electrons and holes are the same. Thus

$$(R_0A)_{\text{GR}} = \frac{V_{bi}}{qn_i w V_{th}\sigma N_f}. \tag{5b}$$

2.3. The tunnelling mechanism

Despite no net tunnelling current in a detector at zero bias, the R_0A product for tunnelling exists for a small voltage swinging about zero. Two kinds of tunnelling current, the direct and indirect tunnelling current, cross the junction [16]. However, because the probability for indirect tunnelling is much lower than that for direct tunnelling, we only consider direct tunnelling in GaInAsSb detectors.

The R_0A product due to tunnelling is defined by [10, 16]

$$(R_0A)_{\text{tunnel}} = \frac{kT}{CT_t(E_n + E_p)^2} \tag{6a}$$

where $C = qm^*/8\pi^2\hbar^3$ is a constant. The terms E_n and E_p are the positions of Fermi levels on each side of the junction and T_t is the tunnelling probability determined by the potential barrier shape. Two kinds of potential barriers, namely triangular and parabolic barriers, are often considered. For a triangular barrier, the probability is given by

$$T_{t1} = \exp\left(-\frac{4\sqrt{2m^*}E_g^{3/2}}{3q\hbar\varepsilon}\right) \tag{6b}$$

and for a parabolic barrier

$$T_{t2} = \exp\left(-\frac{\pi\sqrt{m^*}E_g^{3/2}}{2\sqrt{2}q\hbar\varepsilon}\right) \tag{6c}$$

where $\varepsilon = V_{bi}/w$ is the built-in field through the depletion region.

2.4. The quantum efficiency

Under the condition of low injection and an abrupt junction in a one-dimensional model, the quantum efficiency of GaInAsSb detectors from the three regions (η_n, η_p, η_{dr}), two neutral regions and a spatial charge one, and the total one (η) are shown as follows [12, 17]:

$$\begin{aligned}\eta_n = \frac{(1-r)\alpha L_h}{\alpha^2 L_h^2 - 1}\Bigg\{&\left[\alpha L_h + r_h - \mathrm{e}^{-\alpha(t-x_n)}\right.\\ &\times\left.\left[r_h\cosh\left(\frac{t-x_n}{L_h}\right) + \sinh\left(\frac{t-x_n}{L_h}\right)\right]\right]\\ &\times\left[r_h\sinh\left(\frac{t-x_n}{L_h}\right) + \cosh\left(\frac{t-x_n}{L_h}\right)\right]^{-1}\\ &-\alpha L_h\,\mathrm{e}^{-\alpha(t-x_n)}\Bigg\}\end{aligned} \tag{7a}$$

$$\begin{aligned}\eta_p = \frac{(1-r)\alpha L_e}{\alpha^2 L_e^2 - 1}\,\mathrm{e}^{-\alpha(t+x_p)}\Bigg\{&\left[(r_e - \alpha L_e)\,\mathrm{e}^{-\alpha(d-x_p)}\right.\\ &\left.-r_e\cosh\left(\frac{d-x_p}{L_e}\right) - \sinh\left(\frac{d-x_p}{L_e}\right)\right]\\ &\times\left[\cosh\left(\frac{d-x_p}{L_e}\right) + r_e\sinh\left(\frac{d-x_p}{L_e}\right)\right]^{-1} + \alpha L_e\Bigg\}\end{aligned} \tag{7b}$$

$$\eta_{\text{dr}} = (1-r)(\mathrm{e}^{-\alpha(t-x_n)} - \mathrm{e}^{-\alpha(t+x_p)}) \tag{7c}$$

$$\eta = \eta_p + \eta_n + \eta_{\text{dr}} \tag{7d}$$

where α is an absorption coefficient, $r = 0.35$, the reflection coefficient at the front surface, and other parameters have the same definitions as those in equation (3).

3. Calculation results and discussion

The calculations have been performed on an n–p $Ga_{0.8}In_{0.2}As_{0.19}Sb_{0.81}$ PV detector operated at 300 K and 2.5 μm wavelength. The dependence of GaInAsSb alloy parameters on the compositions x and y are taken from [8]. For practical calculation, the hole mobility was fixed to be $\mu_p = 240$ cm^2 V^{-1} s^{-1} in the p region, and the electron one to be $\mu_e = 1000$ cm^2 V^{-1} s^{-1} in the n region [18]. In addition, the incident light with wavelength 2.48 μm close to the intrinsic absorption edge in the $Ga_{0.8}In_{0.2}As_{0.19}Sb_{0.81}$

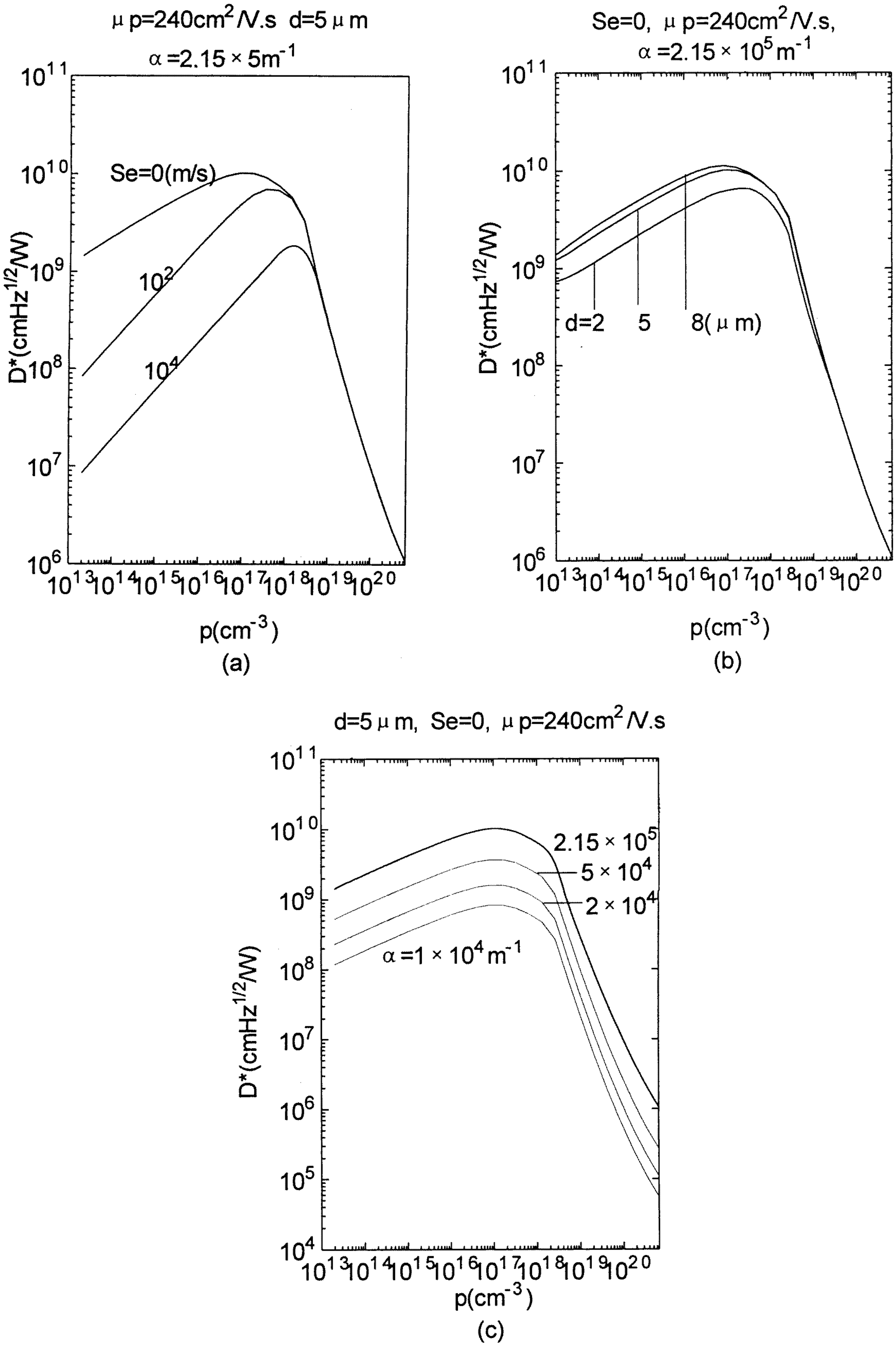

Figure 3. The detectivity versus the p-side carrier concentration (p) with (a) the back-surface recombination velocity (S_e); (b) the p-side width (d); (c) the absorption coefficient (α) as a parameter: $S_p = 0$, $t = 0.5\ \mu$m, $n = 10^{18}$ cm^{-3}, $\sigma N_f = 0.1$ cm^{-1}, $\mu_e = 1000$ cm^2 V^{-1} s^{-1} and $\mu_p = 240$ cm^2 V^{-1} s^{-1}.

alloy is assumed to be injected from the n region then passes the depletion region and finally reaches the p region. Dependent on the incident light energy, the absorption coefficient is taken as $\alpha = 2.15 \times 10^5$ m^{-1} [19]. In general,

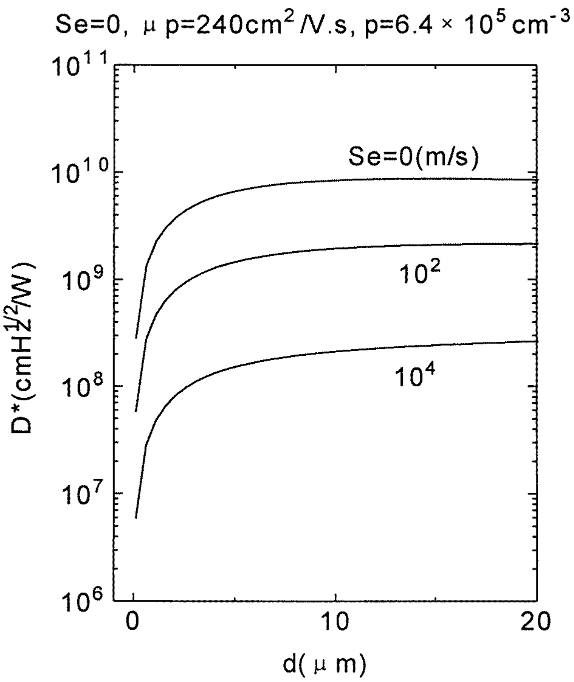

Figure 4. The detectivity versus the p-side width (d) with the back-surface recombination velocity (S_e) as a parameter. Other parameters are the same as those in figure 3.

the capture cross section is assumed to be about 10^{-15} cm^2 [13]. We also assume that the surface recombination velocities on both sides of the detector will yield large electrical reflecting conditions for the holes and electrons respectively.

In this calculation, except for mobilities, other parameters include the R_0A product and the detectivity, such as carrier concentration, widths, surface recombination velocities in the p and n regions and the material absorption coefficient.

$(R_0A)_{\text{total}}$ and the R_0A product components, due to the Auger and radiative mechanisms, the generation–recombination mechanism and the direct tunnelling mechanism have been plotted versus the p-side carrier concentration in figure 1 from equations (2) to (7) respectively, under the condition of $t = 0.5$ μm, $d = 5$ μm, $S_e = S_p = 0$, $n = 10^{18}$ cm^{-3} and $N_f = 10^{14}$ cm^{-3}. Because $(R_0A)_{\text{GR}} \propto 1/\sigma N_f$ in equation (5), we just show the σN_f product as a parameter. D^* in figures 1(a) and (b) corresponds to the triangular and parabolic potential barriers. From figure 1 we can see that

(i) The tunnelling influence appears in $p > 10^{18}$ cm^{-3} because one necessary condition for obtaining tunnelling current is that both n- and p-type semiconductor materials must be degenerate. For $Ga_{0.8}In_{0.2}As_{0.19}Sb_{0.81}$ material, the degeneracy state is at $p > 10^{18}$ cm^{-3} and $n > 10^{16}$ cm^{-3}. On increasing the p-side carrier concentration, $(R_0A)_{\text{tunnel}}$ sharply drops.

(ii) Comparing the two parts of figure 1, it is easy to find that when $p > 10^{18}$ cm^{-3}, the performance of $(R_0A)_{\text{total}}$ is limited by the Auger mechanism on the triangular barrier and by the tunnelling mechanism on the parabolic barrier.

(iii) When $p < 10^{16}$ cm^{-3}, $(R_0A)_{\text{total}}$ is determined by $(R_0A)_{\text{GR}}$. In the range of 10^{16} cm^{-3} $< p <$ 10^{18} cm^{-3}, all of the R_0A product components except for $(R_0A)_{\text{tunnel}}$ contribute to $(R_0A)_{\text{total}}$, and a peak appears at the p-side carrier concentration about 10^{17} cm^{-3}.

Figure 2 shows that the dependence of $(R_0A)_{\text{total}}$ and the R_0A product components on the n-side carrier concentration for various values of the σN_f product for an n–p $Ga_{0.8}In_{0.2}As_{0.19}Sb_{0.81}$ detector, with the same parameters as in figure 1 except for $p = 6.4 \times 10^{16}$ cm^{-3} instead of $n = 10^{18}$ cm^{-3}. In the low p-side carrier concentration, the degeneracy state does not appear so that no tunnelling mechanism influences $(R_0A)_{\text{total}}$. Because of $D^* \propto [(R_0A)_{\text{total}}]^{1/2}$ in equation (1) and $(R_0A)_{\text{GR}} \propto 1/\sigma N_f$ in equation (5), it is an inevitable outcome that $(R_0A)_{\text{total}}$ will be increased and will then improve D^* if the σN_f product is reduced. A similar result is also obtained in the relation between $(R_0A)_{\text{total}}$ and the p-side carrier concentration for various values of the σN_f product. The electron or hole trap densities N_f can be reduced by lowering the concentration of native defects and foreign impurities, which is achieved by improving the growth technique to reach optimization and by progress in purification of material to improve interface qualities [11].

In the following, we discuss the influence of material parameters on the detectivity. Because similar results are shown in figure 1 for different shapes of potential barrier, we only give the results for a parabolic barrier which is usually used in practical application.

From equations (2) to (7), we can find that the quantum efficiency and the R_0A product components are associated with the carrier concentrations in the p and n regions. In addition, the quantum efficiency, $(R_0A)_{\text{Auger}}$ and $(R_0A)_{\text{rad}}$ depend on the surface recombination velocities and the widths of these regions. Moreover, the quantum efficiency is a function of the absorption coefficient determined by the incident light energy; $(R_0A)_{\text{GR}}$ is in inverse proportion to the σN_f product.

Figure 3 shows the dependence of D^* on the p-side carrier concentration with the back-surface recombination velocity S_e, the width of the p region d and the absorption coefficient α as parameters, under the condition of $n = 10^{18}$ cm^{-3}, $t = 0.5$ μm, $S_p = 0$ and $\sigma N_f = 0.1$ cm^{-1}. A similar phenomenon appears in the three parts of figure 3. D^* drops sharply because of the influence of tunnelling in the range of $p > 10^{18}$ cm^{-3}. Comparing figure 1(b) with figure 3, it is found that the depicted shape of D^* is similar to that of $(R_0A)_{\text{total}}$. From this phenomenon, we can draw a conclusion that the shape of D^* is determined by $(R_0A)_{\text{total}}$. In the range of $p < 10^{18}$ cm^{-3}, D^* is determined by the Auger mechanism, radiative mechanism and quantum efficiency in figures 3(a) and 3(b), but rather by the quantum efficiency in figure 3(c). In addition, D^* appears as a peak and then decreases with decreasing p-side carrier concentration. This peak will rise and shift to the low p-side carrier concentration with decreasing back-surface recombination velocity in figure 3(a), but with increasing the p-side width in figure 3(b) and absorption coefficient in figure 3(c). In order to find the greatest thickness of the p region for the optimal D^*, figure 4 shows

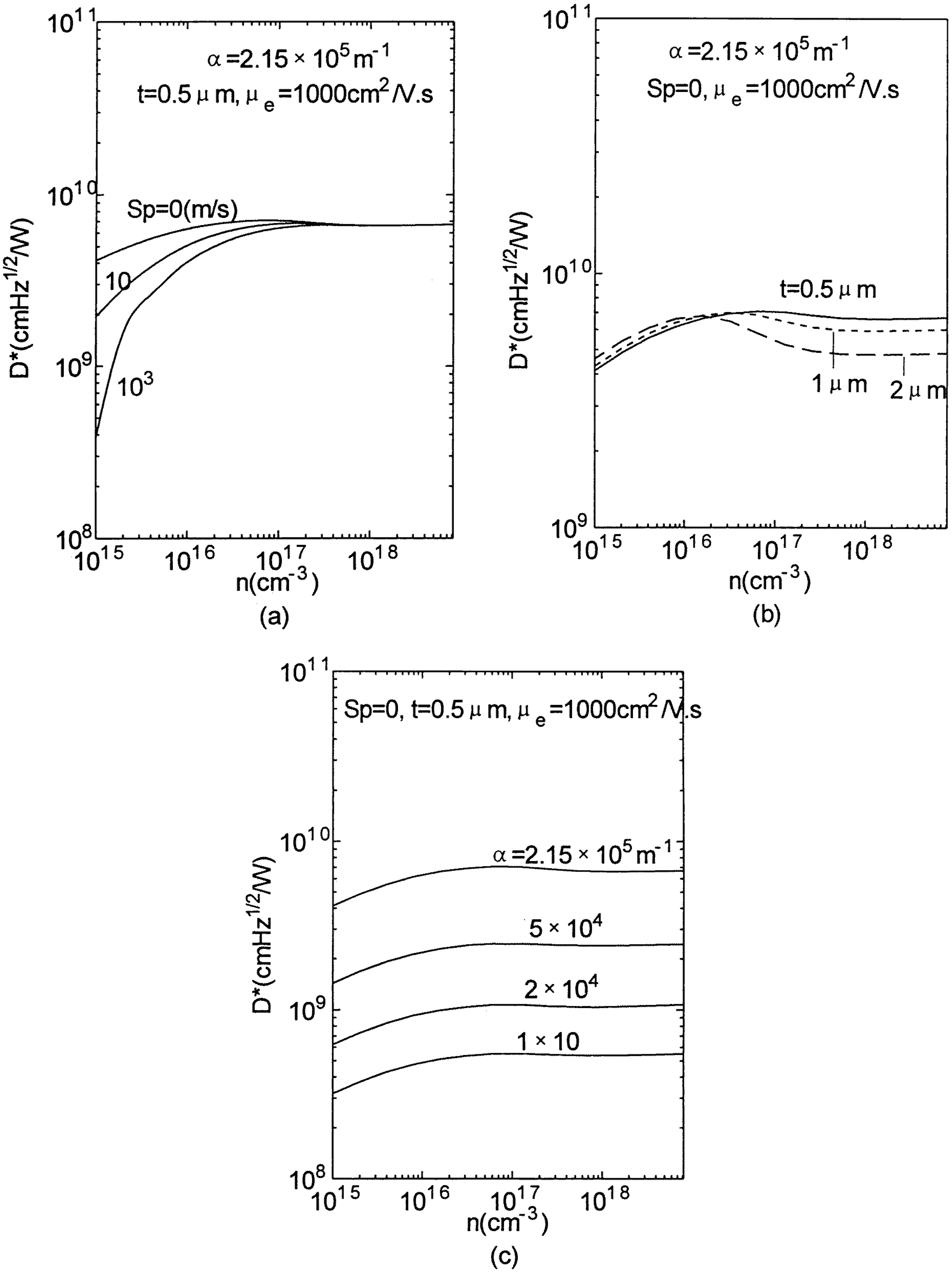

Figure 5. The detectivity versus the n-side carrier concentration (n) with (a) the front-surface recombination velocity (S_p); (b) the n-side width (t); (c) the absorption coefficient (α) as a parameter: S_e = 0, d = 5 μm, $p = 6.4 \times 10^{15}$ cm^{-3}, σN_f = 0.1 cm^{-1}, μ_e = 1000 cm^2 V^{-1} s^{-1} and μ_p = 240 cm^2 V^{-1} s^{-1}.

D^* as a function of the p-side width for $p = 6.4\times10^{15}$ cm^{-3} and with the other parameters the same as in figure 3. D^* in figure 4 reaches a saturated value with an infinite thickness of the p region. However, in [8], to obtain high D^* required reducing the p-side width with an assumption of $\eta = 100\%$ and only considering the Auger mechanism. These differences are caused by considering the quantum efficiency in this paper because the quantum efficiency reaches a saturated value with infinite thickness of the p-side width, dependent on results of [20]. It is clearly indicated that the quantum efficiency will have a great effect on the detectivity. In general, the quantum efficiency cannot be neglected in calculation.

Figure 5 shows D^* versus the n-side carrier concentration with the front-surface recombination velocity S_p, n-side width t and absorption coefficient α as parameters, under the condition of $p = 6.4 \times 10^{15}$ cm^{-3}, $d = 5$ μm, $S_e = 0$, $\sigma N_f = 0.1$ cm^{-1}. From figure 5, we find that the maximal D^* is almost fixed in the range of $n > 10^{17}$ cm^{-3}, which can be explained from figure 2. In figure 2, when the σN_f product is fixed, $(R_0A)_{\mathrm{total}}$ is mainly influenced by $(R_0A)_{\mathrm{GR}}$, and then makes D^* depend on $(R_0A)_{\mathrm{GR}}$. D^* in figures 5(a) and 5(c) is similar to that in figures 3(a) and 3(c) respectively. To obtain a high D^* requires not only a reduction in the front surface recombination velocity S_p but also a reduction in the back one S_e, while D^* will be improved by increasing the absorption coefficient. In [19], the absorption coefficient is dependent on the incident light energy ($h\nu$), $\alpha \propto (1/h\nu - E_g/h\nu^2)^{1/2}$. Substituting this equation into equation (7), the calculated result shows that the incident light energy should be decreased to the band edge absorption in order to get the maximal D^*. The result in figure 3(b) is completely opposite to that in figure 5(b), where decreasing the n-side width will result in high D^*.

4. Conclusion

Calculation and analysis of the effect of material parameters of a $Ga_{0.8}In_{0.2}As_{0.19}Sb_{0.81}$ IR PV detector on the R_0A product and the detectivity at 300 K has been carried out by considering the quantum efficiency and the four fundamental noise mechanisms in the p–n junction such as the Auger and radiative mechanisms in the p and n regions, the generation–recombination mechanism in the depletion region and the tunnelling mechanism through the p–n junction. The results are shown as follows:

(i) Following the above consideration, the figured shape of D^* is mainly determined by the R_0A product and D^* has been much affected by the quantum efficiency.

(ii) To obtain high detectivity requires an incident light energy near the GaInAsSb band edge energy.

(iii) A peak in D^* appears in the dependence of D^* on the p-side carrier concentration. The peak rises and shifts to the low p-side concentration with decreasing back-surface recombination velocity and with an infinite thickness of the p region.

(iv) In the dependence of D^* on the n-side carrier concentration, the detectivity remains almost constant in the range of $n > 10^{17}$ cm^{-3} because of the main influence of the G–R mechanism. Decreasing the front surface recombination velocity and the n-side width will improve the detectivity.

(v) In practical application, the p-side carrier concentration is required to be near the intrinsic carrier concentration, thus the tunnelling mechanism can be neglected. In the process of material preparation and growth, the electron or hole trap densities can be reduced to a minimum in order to improve the detectivity.

Acknowledgment

This paper is supported by the National Advanced Materials Committee of China (NAMCC).

References

[1] Xu J and Tacke M 1992 *Infrared Phys.* **33** 151
[2] Young P M, Grein C H, Ehrenreich H and Miles R H 1993 *J. Appl. Phys.* **74** 4774
[3] Zhang B, Jin Y, Zhou T, Jiang H, Ning Y and Li S 1996 *Mater. Res. Soc. Symp. Proc.* **415** 31
[4] Aardvark A, Allogho G G and Bougnot G 1993 *Semicond. Sci. Technol.* **8** (1S) S380
[5] Srivastave A K, Dewinter J C, Caneau C, Pollack M A and Zysdind J L 1986 *Appl. Phys. Lett.* **48** 903
[6] Rogalski A, Ciupa R and Larkowski W 1996 *Solid State Electron.* **39** 1593
[7] White A M 1986 *Infrared Phys.* **26** 317
[8] Tian Y, Zhou T, Zhang B and Jin Y 1998 *Opt. Eng.* **37** 1754
[9] Piotrowski J, Gawron W and Djuric Z 1994 *Opt. Eng.* **33** 1413
[10] Johnson M R, Chapman R A and Wrobel J S 1975 *Infrared Phys.* **15** 317
[11] Peterson P E 1981 *Semiconductors and Semimetals* vol 18 (New York: Academic) p 201
[12] Rogalski A and Rutkowski J 1982 *Infrared Phys.* **22** 199
[13] Yan J and Hu X 1992 *Proc. SPIE* **1685** 285
[14] Rogalsik A and Orman Z 1985 *Infrared Phys.* **25** 551
[15] Rogalsik A 1988 *Infrared Phys.* **28** 139
[16] Sze S M 1981 *Physics of Semiconductor Devices* 2nd edn (New York: Wiley) p 513
[17] Rosenfeid D and Bahir G 1992 *J. Appl. Phys.* **72** 3034
[18] Li Z A, Zhong J Q and Zheng Y L 1995 *J. Crystal Growth* **150** 1375
[19] Moss T S, Burrell G J and Ellis B 1973 *Semiconductor Opto-electronics* (London: Chapel River Press) p 48
[20] Tian Y, Zhou T, Zhang B, Jiang H and Jin Y *J. SPIE* **3533** 160